

Dissipation-assisted preparation of steady spin-squeezed states of SiV centersJia-Qiang Chen, Yi-Fan Qiao, Xing-Liang Dong, Xin-Lei Hei, and Peng-Bo Li ^{*}*Shaanxi Province Key Laboratory of Quantum Information and Quantum Optoelectronic Devices, School of Physics, Xi'an Jiaotong University, Xi'an 710049, China*

(Received 8 September 2020; accepted 21 December 2020; published 7 January 2021)

We propose an efficient scheme for generating spin-squeezed states at steady state in a spin-mechanical hybrid system, where an ensemble of SiV centers is coupled to a strongly damped nanomechanical resonator. We show that there exists a collective steady state in the system, which is exactly formed by the collective spin states plus the zero excitation state of the mechanical mode. The generation of the steady spin-squeezed state is based on a dissipative quantum dynamical process in which the mechanical dissipation plays a positive role but without destroying the target state. We demonstrate that the spin-squeezed steady state can be deterministically prepared via dissipative means, with the optimal spin squeezing up to $4/N$ in the ideal case, where N is the number of spins. This work provides a promising platform for quantum information processing and quantum metrology.

DOI: [10.1103/PhysRevA.103.013709](https://doi.org/10.1103/PhysRevA.103.013709)**I. INTRODUCTION**

Spin-squeezed states are quantum-correlated states where the fluctuation of one component of the total spin is suppressed below the standard quantum limit. It has been proven that spin-squeezed states are closely related to entangled states [1–5], which lie at the heart of quantum information [6–8] and quantum metrology [9–14]. For these reasons, various schemes for generating spin-squeezed states have been proposed, for instance, the schemes based on nondemolition measurements [15–18], interactions with squeezed light [19–21], and nonlinear interactions [22–24]. In particular, spin squeezing using the one-axis twisting model has been realized in experiments [25]. Despite the exciting progress, it still faces enormous challenges to generate spin-squeezed states. Specifically, due to the disturbance of the environment, most of these spin-squeezed states are temporary and fragile. Recent works on the generation of target states by “quantum reservoir engineering” [26–30] provide us an avenue for investigating spin squeezing. By appropriately designing the interactions with the reservoir, the dissipation can play a positive role in steering a system into the target state.

Solid defects in diamond including nitrogen-vacancy (NV) [31–42], silicon-vacancy (SiV) [43–53], and germanium-vacancy (GeV) [54] color centers have been extensively studied in recent years. They consist of a substitutional impurity atom replacing the carbon atom and adjacent to vacancies. The color center exhibits excellent optical properties, which makes it easy to manipulate and detect [55–58]. More importantly, it has long coherence time [59–62], which can be used as an excellent qubit and a weak signal detector [63–65]. In addition, the color center embedded in a solid-state device is sensitive to the crystal strain, thus giving rise to a coupling with the mechanical mode. Hybrid systems directly

mediated by crystal strain do not require extra structures, thus avoiding the emergence of extra decoherence. Single-crystal diamond, with desirable optical and mechanical properties, is a natural carrier of color centers. Spin-mechanical hybrid quantum systems based on color centers in diamond have been used to produce spin-squeezed states [66–69]. Although mechanical resonators can achieve high quality factors [70–72] with the great progress of nanofabrication techniques, the produced quantum state is still inevitably spoiled by dissipation and decoherence. Therefore, it is highly desirable to prepare persistent and high-quality spin-squeezed states. Note that dissipation-assisted schemes for spin squeezing have been investigated in cavity QED [29] and photonic waveguide systems [36]. However, the spin-phononic hybrid system we considered is fundamentally different from the photonic system. The solid-state phononic device could have important applications in all-phonon quantum information processing and quantum metrology.

In this work, we propose an efficient scheme to generate spin-squeezed states at steady state in a hybrid system, where an ensemble of SiV centers is coupled to a nanomechanical resonator by crystal strain. Because of the excellent optical and strain response of the ground states of the SiV center, it is possible to design two pairs of Raman processes. In the case of large detunings, we can adiabatically eliminate the high energy levels, thus obtaining the desired interactions. We first show that the system possesses a steady squeezed state with no phonon excitations. Under the condition of large dissipations for the mechanical resonator, the mechanical mode will continuously absorb energy from the SiV centers and subsequently decay back to its ground state, steering the spins into a steady squeezed state. This process is verified by numerical simulations. It is important to note that this process does not depend on the initial state of the system. Consider the more realistic case where there exists spin dephasing of SiV centers, and the system gives rises to suppressed spin squeezing. Then, we consider the case of a large number of spins via analytic

^{*}lipengbo@mail.xjtu.edu.cn

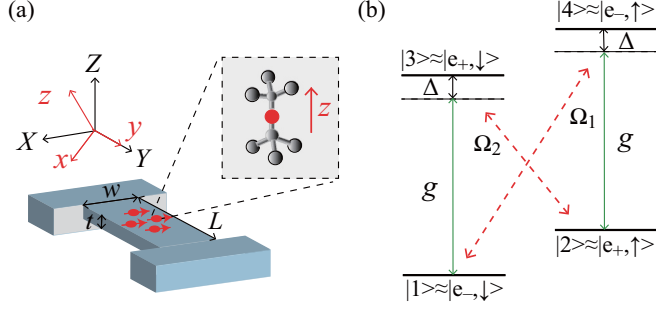


FIG. 1. (a) A diamond nanomechanical resonator with an ensemble of embedded SiV centers. The length, width, and thickness of the beam are L , w , and t , respectively. Local perpendicular strain induced by the bending of the beam couples the SiV centers to the mechanical oscillator. There are two sets of coordinates: (x, y, z) corresponds to the internal basis of the SiV center and (X, Y, Z) corresponds to the axes of the beam. (b) The level structure of the ground state of a SiV center. Two time-dependent microwave driving fields induce the Raman processes between $|3\rangle \leftrightarrow |2\rangle$ and $|4\rangle \leftrightarrow |1\rangle$.

methods. Ideally, by choosing the appropriate parameters, the spin squeezing can be up to the magnitude of $4/N$. In the presence of spin dephasing, the squeezing is suppressed. When the particle number N increases, the effect of spin dephasing will be reduced so that the spin squeezing is close to the ideal case. This work presents a useful proposal for generating spin-squeezed states via dissipative means, which may bring abundant applications in quantum information processing and quantum sensing.

II. THE MODEL

As illustrated in Fig. 1(a), the setup under consideration is realized by a doubly clamped nanobeam with an ensemble of embedded SiV centers. Here the diamond samples used in this study have a [001]-oriented top surface, and the beam is along the [110] direction (Y axis). Thus, there are four possible orientations of SiVs— $[111]$, $[\bar{1}\bar{1}1]$, $[1\bar{1}1]$, and $[\bar{1}11]$ —in a diamond crystal. We choose the SiVs in the $z \parallel [1\bar{1}1]$ direction, and the total Hamiltonian is given by

$$H = H_{\text{SiV}} + H_r + H_1 + H_d, \quad (1)$$

where the individual terms represent the Hamiltonian of the SiV centers, the mechanical mode of the diamond beam, the strain coupling of the SiV centers to the mechanical mode, and the classical driving, respectively.

For the SiV center, the electronic ground states consist of four spin-orbit degenerate states $|e_x, \downarrow\rangle$, $|e_x, \uparrow\rangle$, $|e_y, \downarrow\rangle$, and $|e_y, \uparrow\rangle$, with spin $S = 1/2$. In the presence of an external magnetic field $\vec{B} = B\vec{z}$, the level structure is affected by the spin-orbit coupling (SOC), the Jahn-Teller (JT) effect, and the Zeeman effect. Thus the Hamiltonian of the SiV center is given by

$$H_{\text{SiV}} = -\lambda_{\text{SOC}}\vec{L} \cdot \vec{S} + H_{\text{JT}} + f\gamma_L B L_z + \gamma_S B S_z. \quad (2)$$

Here, γ_L and γ_S are the orbital and spin gyromagnetic ratios, respectively. The spin-orbit coupling with the strength $\lambda_{\text{SOC}}/2\pi \simeq 45$ GHz [73] is much stronger than the other terms. Therefore, we first consider the spin-orbit coupling

and treat the JT interaction and Zeeman interaction as disturbances. In the above basis, as the projections of angular momentum L_x, L_y vanish, the first term is reduced to $-\lambda_{\text{SOC}}L_z S_z$. The corresponding eigenstates are two doublet states $|e_-, \downarrow\rangle, |e_+, \uparrow\rangle$ and $|e_+, \downarrow\rangle, |e_-, \uparrow\rangle$, where $|e_{\pm}\rangle = (|e_x\rangle \pm i|e_y\rangle)/\sqrt{2}$ are the eigenstates of the orbital angular momentum operator L_z . Due to the JT interaction strength $\Upsilon \ll \lambda_{\text{SOC}}$, we neglect the mixing of energy levels caused by the JT effect and only consider the change of eigenenergy $\omega = \sqrt{\lambda_{\text{SOC}}^2 + 4\Upsilon^2}$. As the orbital Zeeman interaction is suppressed by $f \approx 0.1$, it can be neglected and the Zeeman effect simply splits the spin states with $\omega_B = \gamma_S B$. Thus, the Hamiltonian for a single SiV center reads [67,73]

$$H_{\text{SiV}} = \omega_B |2\rangle\langle 2| + \omega |3\rangle\langle 3| + (\omega + \omega_B) |4\rangle\langle 4|. \quad (3)$$

Besides, we add two controlled fields $\Omega_{1/2}$ with frequencies $\omega_{1/2}$ to drive the transitions $|1\rangle, |2\rangle \rightarrow |4\rangle, |3\rangle$, respectively. So, the corresponding Hamiltonian is given by

$$H_d = \Omega_1 |4\rangle\langle 1| e^{-i\omega_1 t} + \Omega_2 |3\rangle\langle 2| e^{-i\omega_2 t} + \text{H.c.} \quad (4)$$

For the mechanical resonator, we choose a doubly clamped diamond beam with a length L , width w , and thickness t , satisfying $L \gg w, t$. In the case of small beam displacements, the strain $\epsilon = \epsilon_0(a + a^\dagger)$ is linear, where ϵ_0 is strain induced by the zero-point motion of the beam, and $a^\dagger(a)$ is the creation (annihilation) operator for the phonon mode with frequency ω_0 . The corresponding Hamiltonian is

$$H_r = \omega_0 a^\dagger a. \quad (5)$$

The strain results in the mixture of the orbital states [73,74] (see Appendix A). In the rotating-wave approximation, the Hamiltonian for the strain coupling reads

$$H_1 = g(a^\dagger J_- + a J_+), \quad (6)$$

where $J_- = (J_+)^{\dagger} = |1\rangle\langle 3| + |2\rangle\langle 4|$ is the spin-conserving lowering operator. Finally, we combine the Hamiltonian of the SiV and mechanical mode into the free Hamiltonian $H_0 = H_{\text{SiV}} + H_r$.

The key idea of this scheme is to design an appropriate interaction and bring the system into the desired state by means of dissipations. We first consider the case where there is only mechanical dissipation. Assuming that the characteristic time scale of the system Hamiltonian is much longer than the reservoir correlation time, the environment can therefore be considered a memoryless reservoir. So we can get the Markovian master equation

$$\frac{d\rho}{dt} = -i[H, \rho] + \kappa \mathcal{D}[a]\rho, \quad (7)$$

where $\mathcal{D}[o]\rho = 2o\rho o^\dagger - \rho o^\dagger o - o^\dagger o \rho$ is the standard Lindblad operator and κ is the mechanical dissipation rate.

To get more insight into the underlying physics, we first apply several transformations to the Hamiltonian to get an effective Hamiltonian. First, in a rotating frame where the classical fields are not oscillating in time just by the following unitary operation $U_R = e^{iRt}$, with

$$R = \omega_1 |4\rangle\langle 4| + \omega_2 |3\rangle\langle 3|, \quad (8)$$

the Hamiltonian for a single SiV center becomes $H^R = U_R H U_R^\dagger + i\dot{U}_R U_R^\dagger$.

Next, in the case of large detunings $\Delta \gg \Omega_{1/2}$, we apply the Schrieffer-Wolff (SW) transformation [75] $U_S = e^S$ with $S = \frac{\Omega_1}{\Delta}(|4\rangle\langle 1| - |1\rangle\langle 4|) + \frac{\Omega_2}{\Delta}(|3\rangle\langle 2| - |2\rangle\langle 3|)$ and $\Delta = \omega + \Delta_B - \omega_1 = \omega - \Delta_B - \omega_2$, which satisfy $[H_0^R, S] = H_d^R$. Keeping the terms up to $(\frac{\Omega_{1/2}}{\Delta})^2$ and ignoring the energy shifts, we obtain

$$H^S = H_0^R + \frac{1}{2}[H_d^R, S] + e^S H_1^R e^{-S}. \quad (9)$$

Finally, turning to the interaction picture by performing the unitary transformation $U_I = e^{-iH_0^R t}$, we have the following Hamiltonian:

$$\begin{aligned} H^I = & ga^+ \left(|1\rangle\langle 3| e^{-i\Delta t} + \frac{\Omega_1}{\Delta} |4\rangle\langle 3| e^{i2\omega_B t} - \frac{\Omega_2}{\Delta} |1\rangle\langle 2| \right) \\ & + ga^+ \left(|2\rangle\langle 4| e^{-i\Delta t} + \frac{\Omega_2}{\Delta} |3\rangle\langle 4| e^{-i2\omega_B t} - \frac{\Omega_1}{\Delta} |2\rangle\langle 1| \right) \\ & + \text{H.c.} \end{aligned} \quad (10)$$

Under the condition $\Delta, \omega_B \gg g, \Omega_{1/2}$, the fast oscillating terms $e^{\pm i\Delta t}$ and $e^{\pm i2\omega_B t}$ can be completely discarded in the rotating-wave approximation. In this case, we implement the standard Raman-transition process with the Λ type and we can eliminate the high energy levels under the large detuning condition. Therefore, the states $|3\rangle, |4\rangle$ can be safely eliminated to obtain the effective Hamiltonian

$$H_{\text{eff}} = \frac{g\Omega}{\Delta} a^+ (\sin\theta \sigma_+ + \cos\theta \sigma_-) + \text{H.c.}, \quad (11)$$

where $\sin\theta = \Omega_1/\Omega$ with $\Omega^2 = \Omega_1^2 + \Omega_2^2$ and $\sigma_- = (\sigma_+)^{\dagger} = |1\rangle\langle 2|$. We further introduce the collective operators $S_- = (S_+)^{\dagger} = \sum_j \sigma_j^-$ and $S_z = \frac{1}{2} \sum_j (|2\rangle_j\langle 2| - |1\rangle_j\langle 1|)$, which satisfy the usual angular momentum commutation relations

$$[S_+, S_-] = 2S_z, [S_z, S_{\pm}] = \pm S_{\pm}. \quad (12)$$

For an ensemble of SiV centers, the sum runs over all SiV centers, and we obtain the total effective Hamiltonian

$$\begin{aligned} H_{\text{eff}} &= \frac{g\Omega}{\Delta} a^+ (\sin\theta S_+ + \cos\theta S_-) + \text{H.c.} \\ &= \frac{g\Omega}{\Delta} a^+ D_- + \text{H.c.}, \end{aligned} \quad (13)$$

where $D_- = D_+^{\dagger} = \sin\theta S_+ + \cos\theta S_-$. The coupling $g\Omega/\Delta$ is therefore an effective Rabi frequency. Meanwhile, the effective master equation is given by

$$\frac{d\rho}{dt} = -i[H_{\text{eff}}, \rho] + \kappa \mathcal{D}[a]\rho. \quad (14)$$

The Hamiltonian H_{eff} describes the transition between the states $\{|1\rangle, |2\rangle\}$, creating or annihilating a phonon, while the Lindblad term will drive the transition from the phonon state $|n\rangle$ to $|n-1\rangle$. Hence, the combined effect of the unitary and dissipative dynamics drives the system to the state $|\Psi\rangle = |\psi\rangle|0\rangle$, i.e., the tensor product of the steady state $|\psi\rangle$ of SiV centers and the phonon vacuum state $|0\rangle$. Since the steady state satisfies $d\rho/dt = 0$, the steady state of SiV centers should obey the equation

$$D_-|\psi\rangle = 0. \quad (15)$$

Assuming the total spin of the system as $S = N/2$, one can expand the steady state in the basis of the eigenstates of

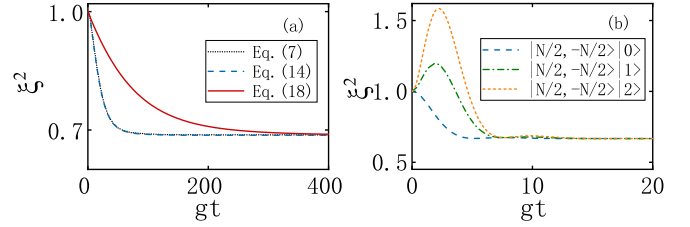


FIG. 2. (a) The spin-squeezing parameter calculated from Eqs. (7), (14), and (18) with $N = 4$ and $\kappa = 0.5g$. The initial state is that all the SiV centers are in the state $|1\rangle$ and the mechanical mode is in the vacuum state. (b) The spin-squeezing parameter from Eq. (14) for different initial states, where $N = 100$ and $\kappa = g$. The other parameters are $\Delta = 20g$, $\Omega = g$, and $\tan\theta = 0.2$.

S_z as $|\psi\rangle = \sum_m c_m |S = N/2, m_s = -N/2 + m\rangle$. By solving Eq. (15), we get the recursion relation between c_m and c_{m+2} . Assuming $c_1 = 0$, we only have the even terms left:

$$c_{m=2n} = (-1)^n \tan^n \theta \binom{N/2}{n} \binom{N}{2n}^{-1/2} c_0. \quad (16)$$

Here $\binom{A}{B} = \frac{A!}{B!(A-B)!}$ are the binomial coefficients and the normalization condition of the state $\sum_m |c_m|^2 = 1$ determines the value of c_0 . Note that the mean spin of the steady state is along the $-z$ direction, and the fluctuation (ΔS_x^2) is suppressed. This is exactly the steady spin-squeezed state that we expect. To quantify the degree of squeezing, we use the spin-squeezing parameter introduced by Wineland *et al.* [76,77]. For this system, the spin-squeezing parameter reduces to

$$\xi^2 = \frac{N \langle S_x^2 \rangle}{|\langle S_z \rangle|^2}. \quad (17)$$

III. NUMERICAL SIMULATIONS

If the mechanical dissipation is sufficiently large, the mechanical mode can be adiabatically eliminated. The reduced master equation for the SiV centers is

$$\frac{d\rho_N}{dt} = \gamma \mathcal{D}[D_-]\rho_N, \quad (18)$$

where $\gamma = g^2 \Omega^2 / \Delta^2 \kappa$ is the collective decay rate induced by mechanical dissipation.

Figure 2(a) shows the results given by Eqs. (7), (14), and (18). We can find that the values for the squeezing parameter calculated from the effective Hamiltonian (13) are almost the same as those obtained from Hamiltonian (1), demonstrating the reasonability of adiabatic eliminations of the high energy levels. Furthermore, we find that the squeezing parameter at the steady state is the same for the two cases obtained from Eqs. (14) and (18), respectively. This demonstrates that, in the large-dissipation limit, the phononic degree of freedom can be adiabatically eliminated from the dynamics. Figure 2(b) shows the results for the squeezing parameter obtained from Eq. (14) with different initial states. The system almost simultaneously evolves into the unique steady spin-squeezed state independent of the initial state. Therefore, we can conclude that Eq. (18) approximately equals Eq. (14) in the large-

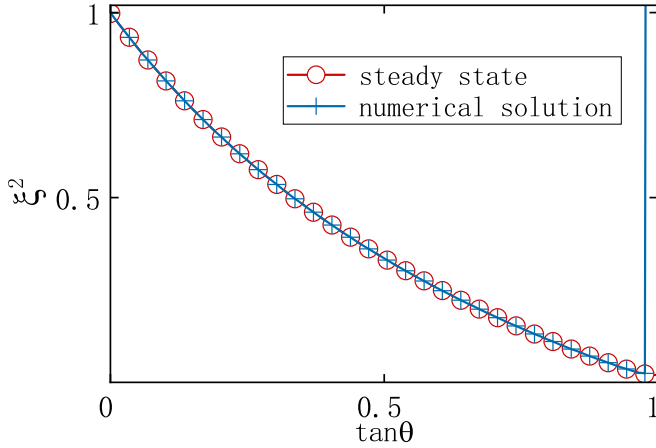


FIG. 3. The spin-squeezing parameter as a function of $\tan \theta$ with $N = 100$ spins.

dissipation limit. Subsequent discussions are uniformly based on Eq. (18).

Assuming the initial state as $|N/2, -N/2\rangle$, we plot the spin-squeezing parameter of the numerical solution [78] compared with the steady state $|\psi\rangle$ as a function of $\tan \theta = \Omega_1/\Omega_2$ in Fig. 3. As expected, the numerical result coincides with the steady state case, indicating that the system evolves to the desired spin-squeezed state.

When $\tan \theta = 0$, the spin-squeezing parameter $\xi^2 = 1$ is the standard quantum limit (SQL) corresponding to a spin coherence state. When $\tan \theta < 1$, the numerical result completely coincides with the steady-state case, and the spin-squeezing parameter is less than 1, indicating that the steady state is a spin-squeezed state. The degree of spin squeezing can be enhanced continuously with the increasing of $\tan \theta$. When $\tan \theta \rightarrow 1$, there is a large deviation between these two cases, since the evolution time of the system will increase rapidly and become infinite at $\tan \theta = 1$. This is due to the fact that the evolution rate is proportional to $\cos(2\theta)$, which can be seen in the following analysis.

As the Hamiltonian commutes with the total spin S^2 and the master equation does not break the conservation of total spin, the total spin will be a constant of motion. Therefore, this steady squeezed state could be produced independent of the z component of the angular momentum. The time evolution of the spin-squeezing parameter for an ensemble of spins with different S_z is shown in Fig. 4. When $t = 0$, all

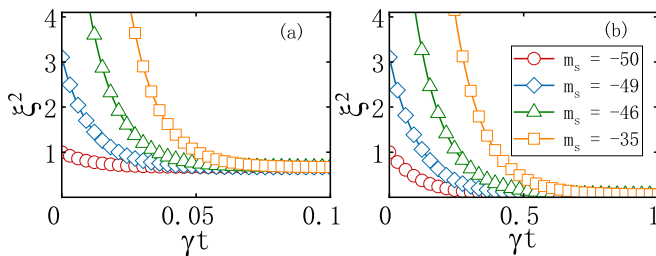


FIG. 4. Time evolution of the squeezing parameter ξ^2 for initial states with different m_s . The parameters are $N = 100$, (a) $\tan \theta = 0.2$ and (b) $\tan \theta = 0.9$.

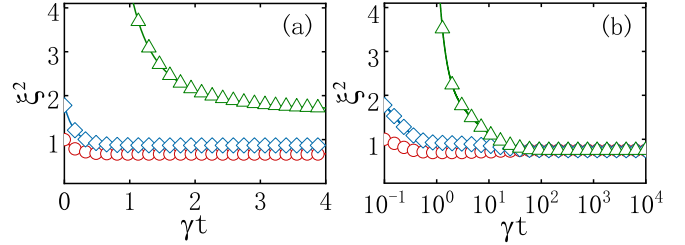


FIG. 5. Time evolution of the squeezing parameter ξ^2 starting from initial states with different total spins. Here the parameters are $N = 8$, $\tan \theta = 0.2$. (a) $\Gamma = 0$. The steady state does depend on the total spins of the initial state. (b) $\Gamma = 0.1\gamma$. The spin dephasing breaks the dependence on the total spin.

the spin-squeezing parameters $\xi^2 \geq 1$, which means that they are not squeezed at the initial time. Then under the assistance of mechanical dissipation, the system starting from different initial states is steered into the same steady squeezed state. It indicates that one total spin corresponds to a common steady state. Compared to Fig. 4(a), Fig. 4(b) gives a reduced squeezing parameter, which is exactly the result shown in Fig. 3. In addition, since the effective decay rate decreases as $\tan \theta$ increases, the evolution time increases.

Now we consider the more realistic case, where the dephasing of SiV centers with a rate Γ is taken into account. The corresponding master equation can be obtained as

$$\frac{d\rho_N}{dt} = \gamma \mathcal{D}[D_-]\rho_N + \Gamma \sum_j \mathcal{D}[\sigma_z^j]\rho_N. \quad (19)$$

Here the Pauli operator $\sigma_z = |2\rangle\langle 2| - |1\rangle\langle 1|$. Such a single-particle process may break the conservation of the total spin. We present the numerical solutions of Eq. (19) with $N = 8$ in Fig. 5. Figure 5(a) shows the time evolution of the squeezing parameter starting from initial states with a different total spin in the case of no dephasing, i.e., $\Gamma = 0$. We find that all the curves decrease continuously with time, but they correspond to a different final state. The bottom curve, corresponding to the case of the total spin $S = N/2$, gives the spin-squeezing parameter $\xi^2 \approx 0.67$.

In Fig. 5(b), the spin dephasing with the rate $\Gamma = 0.1\gamma$ is taken into account. With the same initial conditions as in Fig. 5(a), the spin-squeezing parameters eventually evolve to the same value, which implies that spin dephasing couples different total spin- S manifolds and the system has a unique steady state independent of the total spins. Compared to Fig. 5(a), the first parts of the curves are remarkably similar, where the collective decay induced by phonon dominates the entire evolution. As time goes on, although the dephasing rate is very small, it still shows a great influence: a steady spin-squeezed state completely independent of the initial state is obtained. If we focus on the case with the total spin $S = N/2$, the existence of spin dephasing reduces the degree of squeezing and seems to compete with the squeezing process caused by the phonon decay. But the dependence of the system on the initial state is completely eliminated. In addition, when using a spin ensemble to prepare the spin squeezing, the degree of squeezing usually increases with the number of particles.

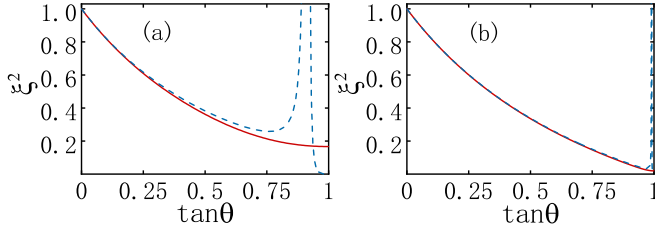


FIG. 6. Spin squeezing ξ^2 for (a) $N = 10$ and (b) $N = 100$ spins. Exact solution of steady state (solid red line) and the analytic approximate solution (dashed blue line).

IV. APPROXIMATE ANALYTIC SOLUTIONS

In order to measure the degree of squeezing in the case of large particle numbers, it is better to find the expression for the spin-squeezing parameter under proper approximations. Note that the spin-squeezing parameter ξ^2 is given by the ratio of $\langle S_x^2 \rangle$ to $\langle S_z \rangle^2$, and we first neglect spin dephasing and solve for the time evolution of $\langle S_x^2 \rangle$ and $\langle S_z \rangle$ from Eq. (18):

$$\frac{d\langle S_z \rangle}{dt} = -2\gamma(\cos^2\theta\langle S_+S_- \rangle - \sin^2\theta\langle S_-S_+ \rangle), \quad (20)$$

$$\frac{d\langle S_x^2 \rangle}{dt} = -2\gamma(\sin\theta - \cos\theta) \times \langle (\sin\theta S_- + \cos\theta S_+)(S_x S_z + S_z S_x) + \text{H.c.} \rangle. \quad (21)$$

Due to the main spin along the $-z$ axis, we use linearization $\langle S_z \rangle \approx -N/2$ and define the small fluctuation as $\delta S_z = S_z + N/2$ to get the simplified equations

$$\frac{d\langle \delta S_z \rangle}{dt} = -2N\gamma \cos(2\theta) \left[\langle \delta S_z \rangle - \frac{\sin^2\theta}{\cos(2\theta)} \right] \quad (22)$$

$$\frac{d\langle S_x^2 \rangle}{dt} = -2N\gamma \cos(2\theta) \left\{ \langle S_x^2 \rangle - \frac{N[1 - \sin(2\theta)]}{4 \cos(2\theta)} \right\}. \quad (23)$$

We can see that they decay exponentially in time, and $\gamma_{\text{eff}} = 2N\gamma \cos(2\theta)$ is the effective rate. When the system reaches steady state, the expectation values of the two operators will not change. We can substitute the steady-state solution of the equations into Eq. (17):

$$\xi^2 = \frac{N^2[1 - \sin(2\theta)] \cos(2\theta)}{[N \cos(2\theta) - 2 \sin^2\theta]^2}. \quad (24)$$

In Fig. 6, we compare this approximate expression with the exact solution of the steady state $|\psi\rangle$. The approximation is valid only if $\tan\theta$ is small. When $\tan\theta$ gets large, the approximate result gradually deviates and even breaks the Heisenberg limit at $\tan\theta = 1$. The deviation comes from two reasons:

(1) With the increase of $\tan\theta$, the probability of occupying the highly excited states increases, as shown in the numerical solution. That means $\langle S_z \rangle \rightarrow 0$, resulting in a rapid increase of spin-squeezing parameter.

(2) At $\tan\theta \sim 1$, the approximate result gives rise to $\langle S_z \rangle = \frac{\sin^2\theta}{\cos(2\theta)} - \frac{N}{2} \rightarrow \infty$, an infinite denominator, which drives the spin-squeezing parameter down to zero.

We plot the time evolution of $\langle \delta S_z \rangle/N$ with different $\tan\theta$ in Fig. 7(a) to obtain the region where the approximation is reasonable and desirable. The linearization that we used

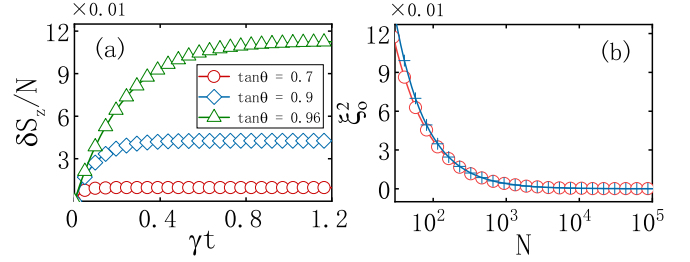


FIG. 7. (a) Time evolution of $\delta S_z/N$ for different $\tan\theta$ with $N = 100$. (b) The optimal squeezing ξ_o^2 as a function of N . The red curve corresponds to the analytic approximate solution with $\tan^2\theta = \frac{N}{N+10}$. The blue curve corresponds to $4/N$.

is equivalent to $\langle \delta S_z \rangle/N \approx 0$. As $\tan\theta$ increases, $\langle \delta S_z \rangle/N$ at the steady state increases so rapidly that the approximation completely fails. Therefore, here we choose $\langle \delta S_z \rangle/N \leq 0.1$ to satisfy the linear approximation. One can get $\tan^2\theta \leq \frac{N}{N+10}$ and verify that the approximate solution is valid in Fig. 6. Although this condition is approximate, it can be verified that $\tan^2\theta = \frac{N}{N+10}$ is close to the region where the minimum value occurs. Therefore, we assume that the spin-squeezing parameter near this region is the optimal parameter that leads to maximal squeezing. The corresponding squeezing parameter ξ_o^2 (red line) is shown in Fig. 7(b). As N increases, the spin-squeezing parameter decreases dramatically and it can be found that it fits well with $\xi_o^2 = 4/N$ (blue line) for very large N .

Finally, we take into account the spin dephasing to study the degree of squeezing in the case of very large N . Once again, by using Eq. (19) we obtain

$$\langle \delta S_z \rangle_\infty = \frac{\sin^2\theta}{\cos(2\theta)}, \quad (25)$$

$$\langle S_x^2 \rangle_\infty = \frac{N N \eta [1 - \sin(2\theta)] + 4}{4 N \eta \cos(2\theta) + 4}, \quad (26)$$

where $\eta = \gamma/\Gamma$ is the single spin cooperativity. Note that the spin-squeezing parameter should be equal to Eq. (24) when $N\eta$ is large. We present the calculation of the spin-squeezing parameter with different η in Fig. 8. We find that the dephasing only slightly affects the spin-squeezing parameter for a wide parameter range. It competes with the squeezing process induced by the mechanical dissipation. However, as the value of $\tan\theta$ increases, the dephasing effect will be significant. The spin-squeezing parameter has a minimum value corresponding to the optimal squeezing in the presence of dephasing.

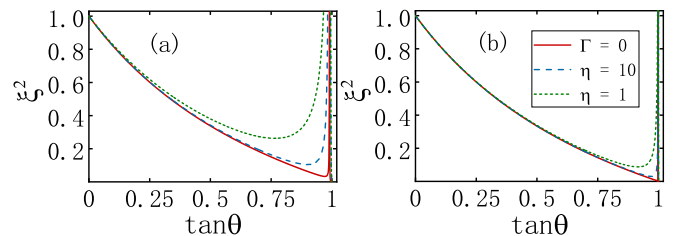


FIG. 8. The analytic approximate solution as a function of $\tan\theta$ in the presence of dephasing for (a) $N = 100$ and (b) $N = 1000$ spins.

By increasing the number of SiV centers and decreasing the dephasing rate, the system will work very well even for large $\tan \theta$.

V. EXPERIMENTAL FEASIBILITY OF THIS SCHEME

In order to examine the feasibility of this scheme in experiment, we now discuss the relevant parameters. For the beam, we consider a single-crystal diamond nanomechanical resonator with dimensions $(L, w, t) = (6.29, 0.5, 0.5) \mu\text{m}$. The material properties are Young's modulus $E \approx 1.05 \text{ TPa}$, mass density $\rho \approx 3500 \text{ kg m}^{-3}$, and Poisson ratio $\nu = 0.2$. As the splitting of the orbital states of SiV centers is about 46 GHz, the corresponding resonance frequency of the bending mode is $\omega_0/2\pi \approx 45.9 \text{ GHz}$. Generally, the SiV centers in a diamond crystal have four different orientations. In the case of static magnetic fields along the $[1\bar{1}1]$ orientation, these four types of SiV centers have different Zeeman splittings. Only the SiV centers in the $[1\bar{1}1]$ orientation resonate with the driving field and are considered while other SiV centers can be neglected due to off resonance. In this case, the coupling between a single SiV center and the mechanical mode is given by $g = (1 + \nu)d\epsilon_0 \approx 2\pi \times 10 \text{ MHz}$.

In addition, we assume the driving field $\Omega_1/2\pi = 6.7 \text{ MHz}$, $\Omega_2/2\pi = 7.4 \text{ MHz}$, i.e., $\Omega/2\pi = 10 \text{ MHz}$, and $\tan \theta = 0.9$. And the detuning $\Delta/2\pi$ in our scheme is about 200 MHz, thus satisfying the condition $\Delta \gg g, \Omega$. The mechanical dissipation rate is $\kappa/2\pi \sim 10 \text{ MHz}$. For a single SiV center, the effective decay rate induced by the mechanical dissipation is $\gamma = g^2\Omega^2/\Delta^2\kappa \sim 2\pi \times 25 \text{ kHz}$. We assume the temperature is $T = 100 \text{ mK}$, and thus the average phonon number is $n \approx 0$, which leads to the correlation time of the thermal reservoir, $t_R \approx \hbar/k_B T$. Since $t_S/t_R \sim 10^3$, the Markovian approximation is justified.

At 100 mK temperature, the spin-dephasing rate of single SiV centers is $\Gamma/2\pi \sim 100 \text{ Hz}$, which means the spin coherence time is $T_2 \sim 10 \text{ ms}$. According to Fig. 4, the time for the system to reach the steady spin-squeezed state is about 40 μs , which is much shorter than the spin coherence time. Experimentally, the SiV center density has reached 8 ppm [79], so it is easy to reach 10^4 color centers in our scheme. In this case, we predict that the spin-squeezing parameter can be up to 4×10^{-4} with the appropriate parameters.

VI. CONCLUSION

In conclusion, we have proposed a scheme to generate a steady spin-squeezed state in a spin-mechanical hybrid system. We find a collective steady state in the system, which is exactly formed by the collective spin states plus the zero excitation state of the mechanical mode. In the case of large detuning, the system of total spin $S = N/2$ can be steered to a steady squeezed state with the assistance of mechanical dissipation. In the ideal case, the squeezing $\xi_o^2 \sim 4/N$ can be achieved. In the presence of spin dephasing, the spin squeezing is reduced. The generation of the steady spin-squeezed state is not dependent on the initial state of the system and the degree of spin squeezing can reach the result in the ideal case as N increases. This spin-mechanical system provides a promising platform for studying the nonclassical state.

ACKNOWLEDGMENTS

This work is supported by the National Natural Science Foundation of China under Grants No. 11774285, No. 92065105 and the Natural Science Basic Research Program of Shaanxi (Program No. 2020JC-02).

APPENDIX A: STRAIN COUPLING

The detailed derivation for the strain coupling between SiV centers and mechanical resonators has been discussed in Refs. [73,74,80]. Here we follow the discussions and present the key results. In what follows, we use two sets of coordinates: the internal basis of the SiV center and the axes of the diamond crystal ($X \parallel [1\bar{1}0]$, $Y \parallel [110]$, $Z \parallel [001]$). There are four possible directions of the color center inlaid on the diamond sample, $[\bar{1}11]$, $[1\bar{1}1]$, $[\bar{1}\bar{1}1]$, and $[111]$, respectively. For a long and thin beam, the bending modes can be described by elasticity theory and Euler-Bernoulli flexure theory. The wave equation for beam deflections of the neutral axis obeys

$$EI \frac{\partial^4 U}{\partial Y^4} = -\rho A \frac{\partial^2 U}{\partial t^2}, \quad (\text{A1})$$

where U represents the beam deflection in the Z direction and Y is along the length of the beam. Here, $E \approx 1.05 \text{ TPa}$ is Young's modulus of diamond, $I = wt^3/12$ is the moment of inertia of the beam, $\rho \approx 3500 \text{ kg m}^{-3}$ is the mass density of diamond, and $A = wt$ is the cross-section area in the transverse plane. Solutions of the above equation for a doubly clamped beam take the form $U_n(t, Y) = u_n(Y)e^{-i\omega_n t}$. According to the boundary conditions $u(0) = u'(0) = u(L) = u'(L) = 0$, $u_n(Y)$ is given by

$$u_n(Y) = \cos k_n Y - \cosh k_n Y - \frac{\cos k_n L - \cosh k_n L}{\sin k_n L - \sinh k_n L} \times (\sin k_n Y - \sinh k_n Y). \quad (\text{A2})$$

The wavenumbers k_n satisfy $\cos k_n L \cosh k_n L = 1$, and the eigenfrequencies are given by

$$\omega_n = k_n^2 \sqrt{\frac{EI}{\rho A}}. \quad (\text{A3})$$

We consider the frequency near 46 GHz, which is obtained when $kL = 67.55$. For small beam displacements, the strain induced by the beam motion is linear: $\epsilon = \epsilon_0(a + a^\dagger)$. Here, ϵ_0 is the strain induced by the beam zero-point motion and a is the annihilation operator of the phonon mode. Assuming that the SiV center is located in the midpoint along the beam and away from the neutral axis of the beam, i.e., $Y = L/2$, $R_0 \approx t/2$, the strain induced by the zero-point motion of the beam is

$$\epsilon_0 = -R_0 \sqrt{\frac{\hbar}{2\rho A L \omega_n}} \frac{\partial^2 u_n(L/2)}{\partial Y^2} \approx 8 \times 10^{-9}. \quad (\text{A4})$$

In the beam's basis, the strain tensor is given by

$$\epsilon_b = \begin{bmatrix} -\nu\epsilon & 0 & 0 \\ 0 & \epsilon & 0 \\ 0 & 0 & -\nu\epsilon \end{bmatrix}, \quad (\text{A5})$$

where $\nu = 0.2$ is the Poisson ratio. Now we need to transform the above strain tensor from the beam's basis into the SiV's basis. For the SiVs oriented along the $[111]$ and $[\bar{1}\bar{1}\bar{1}]$ directions, the transformed strain tensors are

$$\epsilon_{[111]} = \begin{bmatrix} \frac{1}{3}(1-2\nu)\epsilon & 0 & -\frac{\sqrt{2}}{3}(1+\nu)\epsilon \\ 0 & -\nu\epsilon & 0 \\ -\frac{\sqrt{2}}{3}(1+\nu)\epsilon & 0 & \frac{1}{3}(2-\nu)\epsilon \end{bmatrix}, \quad (\text{A6})$$

$$\epsilon_{[\bar{1}\bar{1}\bar{1}]} = \begin{bmatrix} \frac{1}{3}(1-2\nu)\epsilon & 0 & \frac{\sqrt{2}}{3}(1+\nu)\epsilon \\ 0 & -\nu\epsilon & 0 \\ \frac{\sqrt{2}}{3}(1+\nu)\epsilon & 0 & \frac{1}{3}(2-\nu)\epsilon \end{bmatrix}. \quad (\text{A7})$$

For the SiVs oriented along the $[\bar{1}11]$ and $[1\bar{1}\bar{1}]$ directions, the transformed strain tensors are the same:

$$\epsilon_t = \begin{bmatrix} -\nu\epsilon & 0 & 0 \\ 0 & \epsilon & 0 \\ 0 & 0 & -\nu\epsilon \end{bmatrix}. \quad (\text{A8})$$

By projecting the strain tensor onto the irreducible representation of D_{3d} , the strain coupling within the framework of linear elasticity theory can be given by

$$H_{\text{strain}} = \sum_r V_r \epsilon_r, \quad (\text{A9})$$

where r runs over the irreducible representations. It can be shown that the only contributing representations are the one-dimensional representation A_{1g} and the two-dimensional representation E_g . We have

$$\begin{aligned} \epsilon_{A_{1g}} &= t_{\perp}(\epsilon_{xx} + \epsilon_{yy}) + t_{\parallel}\epsilon_{zz}, \\ \epsilon_{E_g} &= d(\epsilon_{xx} - \epsilon_{yy}) + f\epsilon_{zx}, \\ \epsilon_{E_g} &= -2d\epsilon_{xy} + f\epsilon_{yz}, \end{aligned} \quad (\text{A10})$$

where t_{\perp} , t_{\parallel} , d , and f are four strain-susceptibility parameters. It is valid to drop the f terms due to $f/d \sim 10^{-4}$. The effects of these strain components on the electronic states are

described by

$$\begin{aligned} V_{A_{1g}} &= |e_x\rangle\langle e_x| + |e_y\rangle\langle e_y|, \\ V_{E_{gx}} &= |e_x\rangle\langle e_x| - |e_y\rangle\langle e_y|, \\ V_{E_{gy}} &= |e_x\rangle\langle e_y| + |e_y\rangle\langle e_x|. \end{aligned} \quad (\text{A11})$$

Since $V_{A_{1g}}$ is the identity matrix, the $\epsilon_{A_{1g}}$ term only gives rise to the uniform energy shift of all states and can be neglected. Finally, we rewrite the strain Hamiltonian in the basis of $|e_+\rangle$, $|e_-\rangle$:

$$H_{\text{strain}} = d(\epsilon_{xx} - \epsilon_{yy})(L_- + L_+), \quad (\text{A12})$$

where $L_+ = L_-^\dagger = |3\rangle\langle 1| + |2\rangle\langle 4|$ is the orbital raising operator. We find the common form of the coupling for four kinds of SiVs, and the difference is only the strength of the coupling: $g_a = \frac{1}{3}(1+\nu)\epsilon d$ and $g_t = (1+\nu)\epsilon d$ corresponding to ($[111]$, $[\bar{1}\bar{1}\bar{1}]$) and ($[\bar{1}11]$, $[1\bar{1}\bar{1}]$) orientations. Finally, by using a rotating-wave approximation, we get the Hamiltonian in the text:

$$H_{\text{strain}} = gaJ_+ + \text{H.c.}, \quad (\text{A13})$$

where $J_- = (J_+)^{\dagger} = |1\rangle\langle 3| + |2\rangle\langle 4|$ is the spin-conserving lowering operator. For the SiV center in $[\bar{1}11]$, $[1\bar{1}\bar{1}]$ orientations, the coupling strength is

$$g = (1+\nu)\epsilon d \sim 2\pi \times 10 \text{ MHz}. \quad (\text{A14})$$

APPENDIX B: EFFECTS OF MAGNETIC FIELDS

To avoid the nonuniform coupling, we adjust the magnetic field to pick up the color centers in a certain orientation. The static magnetic field $\vec{B} = (B_x, B_y, B_z)$ is represented in the internal coordinate of the four color centers. In the basis of $|e_x, \downarrow\rangle$, $|e_x, \uparrow\rangle$, $|e_y, \downarrow\rangle$, and $|e_y, \uparrow\rangle$, we neglect the small orbital Zeeman effect and the Hamiltonian of the single SiV center is given by

$$H_{\text{SiV}} = \begin{bmatrix} \Upsilon_x + \frac{1}{2}\gamma_S B_z & \frac{1}{2}\gamma_S B_x - \frac{1}{2}i\gamma_S B_y & \Upsilon_y - \frac{1}{2}i\lambda_{\text{SOC}} & 0 \\ \frac{1}{2}\gamma_S B_x + \frac{1}{2}i\gamma_S B_y & \Upsilon_x - \frac{1}{2}\gamma_S B_z & 0 & \Upsilon_y + \frac{1}{2}i\lambda_{\text{SOC}} \\ \Upsilon_y + \frac{1}{2}i\lambda_{\text{SOC}} & 0 & -\Upsilon_x + \frac{1}{2}\gamma_S B_z & \frac{1}{2}\gamma_S B_x - \frac{1}{2}i\gamma_S B_y \\ 0 & \Upsilon_y - \frac{1}{2}i\lambda_{\text{SOC}} & \frac{1}{2}\gamma_S B_x + \frac{1}{2}i\gamma_S B_y & -\Upsilon_x - \frac{1}{2}\gamma_S B_z \end{bmatrix}. \quad (\text{B1})$$

The eigenvalues of the above matrix can be directly solved as

$$E = \pm \sqrt{\Upsilon^2 + \frac{1}{4}\lambda_{\text{SOC}}^2 + \frac{1}{4}\gamma_S^2 B_z^2 \pm \sqrt{\gamma_S^2 B_z^2 (\Upsilon^2 + \frac{1}{4}\lambda_{\text{SOC}}^2) + \frac{1}{4}(\gamma_S^2 B_x^2 + \gamma_S^2 B_y^2)^2}}, \quad (\text{B2})$$

where $\Upsilon = \sqrt{\Upsilon_x^2 + \Upsilon_y^2}$. For example, we choose the direction of the magnetic field along the $[1\bar{1}\bar{1}]$ direction, and the magnitude satisfies $\gamma_S |\vec{B}| = 2\pi \times 20 \text{ GHz}$. For the SiV in the $[1\bar{1}\bar{1}]$ direction, the energy level splittings are

$$\Delta\omega_{41}/2\pi \approx 66 \text{ GHz}, \quad (\text{B3})$$

$$\Delta\omega_{32}/2\pi \approx 26 \text{ GHz}. \quad (\text{B4})$$

For the other three kinds of SiV centers, these values become

$$\Delta\omega'_{41}/2\pi \approx 53 \text{ GHz}, \quad (\text{B5})$$

$$\Delta\omega'_{32}/2\pi \approx 39 \text{ GHz}. \quad (\text{B6})$$

If we choose the frequencies of the driving fields as $\omega_1/2\pi \approx 66 \text{ GHz}$ and $\omega_2/2\pi \approx 26 \text{ GHz}$, only the SiV centers in the $[1\bar{1}\bar{1}]$ direction can be excited, and the other SiV centers are

off resonant with the driving field. Therefore, only the SiV centers in the $[1\bar{1}1]$ direction are selected to participate in the

Raman process. In addition, the orbital splitting for all the color centers is $\omega/2\pi \approx 46$ GHz.

-
- [1] J. Ma, X. Wang, C. P. Sun, and F. Nori, Quantum spin squeezing, *Phys. Rep.* **509**, 89 (2011).
- [2] X. Wang and B. C. Sanders, Spin squeezing and pairwise entanglement for symmetric multiqubit states, *Phys. Rev. A* **68**, 012101 (2003).
- [3] J. K. Korbicz, J. I. Cirac, and M. Lewenstein, Spin Squeezing Inequalities and Entanglement of n Qubit States, *Phys. Rev. Lett.* **95**, 120502 (2005).
- [4] G. Vitagliano, I. Apellaniz, I. L. Egusquiza, and G. Tóth, Spin squeezing and entanglement for an arbitrary spin, *Phys. Rev. A* **89**, 032307 (2014).
- [5] Y. Zhou, B. Li, X.-X. Li, F.-L. Li, and P.-B. Li, Preparing multiparticle entangled states of nitrogen-vacancy centers via adiabatic ground-state transitions, *Phys. Rev. A* **98**, 052346 (2018).
- [6] N. Bigelow, Quantum engineering: Squeezing entanglement, *Nature* **409**, 27 (2001).
- [7] O. Gühne and G. Tóth, Entanglement detection, *Phys. Rep.* **474**, 1 (2009).
- [8] L. Amico, R. Fazio, A. Osterloh, and V. Vedral, Entanglement in many-body systems, *Rev. Mod. Phys.* **80**, 517 (2008).
- [9] J. Appel, P. J. Windpassinger, D. Oblak, U. B. Hoff, N. Kjaergaard, and E. S. Polzik, Mesoscopic atomic entanglement for precision measurements beyond the standard quantum limit, *Proc. Natl. Acad. Sci. U.S.A.* **106**, 10960 (2009).
- [10] A. Louchet-Chauvet, J. Appel, J. J. Renema, D. Oblak, N. Kjaergaard, and E. S. Polzik, Entanglement-assisted atomic clock beyond the projection noise limit, *New J. Phys.* **12**, 065032 (2010).
- [11] V. Petersen, L. B. Madsen, and K. Mølmer, Magnetometry with entangled atomic samples, *Phys. Rev. A* **71**, 012312 (2005).
- [12] K. W. Lee, D. Lee, P. Ovartchaiyapong, J. Minguzzi, J. R. Maze, and A. C. Bleszynski Jayich, Strain Coupling of a Mechanical Resonator to a Single Quantum Emitter in Diamond, *Phys. Rev. Appl.* **6**, 034005 (2016).
- [13] J. F. Barry, J. M. Schloss, E. Bauch, M. J. Turner, C. A. Hart, L. M. Pham, and R. L. Walsworth, Sensitivity optimization for NV-diamond magnetometry, *Rev. Mod. Phys.* **92**, 015004 (2020).
- [14] C. L. Degen, F. Reinhard, and P. Cappellaro, Quantum sensing, *Rev. Mod. Phys.* **89**, 035002 (2017).
- [15] A. Kuzmich, L. Mandel, and N. P. Bigelow, Generation of Spin Squeezing via Continuous Quantum Nondemolition Measurement, *Phys. Rev. Lett.* **85**, 1594 (2000).
- [16] J. Zhang, K. Peng, and S. L. Braunstein, Backaction-induced spin-squeezed states in a detuned quantum-nondemolition measurement, *Phys. Rev. A* **68**, 035802 (2003).
- [17] V. Shah, G. Vasilakis, and M. V. Romalis, High Bandwidth Atomic Magnetometry with Continuous Quantum Nondemolition Measurements, *Phys. Rev. Lett.* **104**, 013601 (2010).
- [18] R. Inoue, S.-I.-R. Tanaka, R. Namiki, T. Sagawa, and Y. Takahashi, Unconditional Quantum-Noise Suppression via Measurement-Based Quantum Feedback, *Phys. Rev. Lett.* **110**, 163602 (2013).
- [19] A. Kuzmich, K. Mølmer, and E. S. Polzik, Spin Squeezing in an Ensemble of Atoms Illuminated with Squeezed Light, *Phys. Rev. Lett.* **79**, 4782 (1997).
- [20] J. Hald, J. L. Sørensen, C. Schori, and E. S. Polzik, Spin Squeezed Atoms: A Macroscopic Entangled Ensemble Created by Light, *Phys. Rev. Lett.* **83**, 1319 (1999).
- [21] M. Fleischhauer and S. Gong, Stationary Source of Nonclassical or Entangled Atoms, *Phys. Rev. Lett.* **88**, 070404 (2002).
- [22] M. Kitagawa and M. Ueda, Squeezed spin states, *Phys. Rev. A* **47**, 5138 (1993).
- [23] B. C. Sanders, Quantum dynamics of the nonlinear rotator and the effects of continual spin measurement, *Phys. Rev. A* **40**, 2417 (1989).
- [24] M. Takeuchi, S. Ichihara, T. Takano, M. Kumakura, T. Yabuzaki, and Y. Takahashi, Spin Squeezing via One-Axis Twisting with Coherent Light, *Phys. Rev. Lett.* **94**, 023003 (2005).
- [25] C. Gross, T. Zibold, E. Nicklas, J. Estève, and M. K. Oberthaler, Nonlinear atom interferometer surpasses classical precision limit, *Nature* **464**, 1165 (2010).
- [26] F. Verstraete, M. M. Wolf, and J. Ignacio Cirac, Quantum computation and quantum-state engineering driven by dissipation, *Nat. Phys.* **5**, 633 (2009).
- [27] B. Kraus, H. P. Büchler, S. Diehl, A. Kantian, A. Micheli, and P. Zoller, Preparation of entangled states by quantum Markov processes, *Phys. Rev. A* **78**, 042307 (2008).
- [28] H. Krauter, C. A. Muschik, K. Jensen, W. Wasilewski, J. M. Petersen, J. I. Cirac, and E. S. Polzik, Entanglement Generated by Dissipation and Steady State Entanglement of Two Macroscopic Objects, *Phys. Rev. Lett.* **107**, 080503 (2011).
- [29] E. G. Dalla Torre, J. Otterbach, E. Demler, V. Vuletic, and M. D. Lukin, Dissipative Preparation of Spin Squeezed Atomic Ensembles in a Steady State, *Phys. Rev. Lett.* **110**, 120402 (2013).
- [30] Q. Z. Hou, C. J. Yang, C. Y. Chen, J. H. An, W. L. Yang, and M. Feng, Preservation of quantum correlation between nitrogen-vacancy-center ensembles by squeezed-reservoir engineering, *Phys. Rev. A* **100**, 032302 (2019).
- [31] P.-B. Li, Z.-L. Xiang, P. Rabl, and F. Nori, Hybrid Quantum Device with Nitrogen-Vacancy Centers in Diamond Coupled to Carbon Nanotubes, *Phys. Rev. Lett.* **117**, 015502 (2016).
- [32] P.-B. Li, Y.-C. Liu, S.-Y. Gao, Z.-L. Xiang, P. Rabl, Y.-F. Xiao, and F.-L. Li, Hybrid Quantum Device Based on NV Centers in Diamond Nanomechanical Resonators Plus Superconducting Waveguide Cavities, *Phys. Rev. Appl.* **4**, 044003 (2015).
- [33] S. Meesala, Y.-I. Sohn, H. A. Atikian, S. Kim, M. J. Burek, J. T. Choy, and M. Lončar, Enhanced Strain Coupling of Nitrogen-Vacancy Spins to Nanoscale Diamond Cantilevers, *Phys. Rev. Appl.* **5**, 034010 (2016).
- [34] M. W. Doherty, N. B. Manson, P. Delaney, F. Jelezko, J. Wrachtrup, and L. C. L. Hollenberg, The nitrogen-vacancy colour centre in diamond, *Phys. Rep.* **528**, 1 (2013).
- [35] M. W. Doherty, F. Dolde, H. Fedder, F. Jelezko, J. Wrachtrup, N. B. Manson, and L. C. L. Hollenberg, Theory of the

- ground-state spin of the NV⁻ center in diamond, *Phys. Rev. B* **85**, 205203 (2012).
- [36] W. Song, W. Yang, J. An, and M. Feng, Dissipation-assisted spin squeezing of nitrogen-vacancy centers coupled to a rectangular hollow metallic waveguide, *Opt. Express* **25**, 19226 (2017).
- [37] P.-B. Li, S.-Y. Gao, H.-R. Li, S.-L. Ma, and F.-L. Li, Dissipative preparation of entangled states between two spatially separated nitrogen-vacancy centers, *Phys. Rev. A* **85**, 042306 (2012).
- [38] D. A. Golter, T. Oo, M. Amezcua, I. Lekavicius, K. A. Stewart, and H. Wang, Coupling a Surface Acoustic Wave to an Electron Spin in Diamond via a Dark State, *Phys. Rev. X* **6**, 041060 (2016).
- [39] J. R. Maze, A. Gali, E. Togan, Y. Chu, A. Trifonov, E. Kaxiras, and M. D. Lukin, Properties of nitrogen-vacancy centers in diamond: The group theoretic approach, *New J. Phys.* **13**, 025025 (2011).
- [40] B. Li, P.-B. Li, Y. Zhou, S.-L. Ma, and F.-L. Li, Quantum microwave-optical interface with nitrogen-vacancy centers in diamond, *Phys. Rev. A* **96**, 032342 (2017).
- [41] P.-B. Li, Y. Zhou, W.-B. Gao, and F. Nori, Enhancing Spin-Phonon and Spin-Spin Interactions Using Linear Resources in a Hybrid Quantum System, *Phys. Rev. Lett.* **125**, 153602 (2020).
- [42] P.-B. Li and F. Nori, Hybrid Quantum System with Nitrogen-Vacancy Centers in Diamond Coupled to Surface-Phonon Polaritons in Piezomagnetic Superlattices, *Phys. Rev. Appl.* **10**, 024011 (2018).
- [43] C. Hepp, T. Müller, V. Waselowski, J. N. Becker, B. Pingault, H. Sternschulte, D. Steinmüller-Nethl, A. Gali, J. R. Maze, M. Atatüre, and C. Becher, Electronic Structure of the Silicon Vacancy Color Center in Diamond, *Phys. Rev. Lett.* **112**, 036405 (2014).
- [44] L. J. Rogers, K. D. Jahnke, M. W. Doherty, A. Dietrich, L. P. McGuinness, C. Müller, T. Teraji, H. Sumiya, J. Isoya, N. B. Manson, and F. Jelezko, Electronic structure of the negatively charged silicon-vacancy center in diamond, *Phys. Rev. B* **89**, 235101 (2014).
- [45] J. N. Becker, J. Görlitz, C. Arend, M. Markham, and C. Becher, Ultrafast all-optical coherent control of single silicon vacancy colour centres in diamond, *Nat. Commun.* **7**, 13512 (2016).
- [46] A. Sipahigil, K. D. Jahnke, L. J. Rogers, T. Teraji, J. Isoya, A. S. Zibrov, F. Jelezko, and M. D. Lukin, Indistinguishable Photons from Separated Silicon-Vacancy Centers in Diamond, *Phys. Rev. Lett.* **113**, 113602 (2014).
- [47] K. D. Jahnke, A. Sipahigil, J. M. Binder, M. W. Doherty, M. Metsch, L. J. Rogers, N. B. Manson, M. D. Lukin, and F. Jelezko, Electron-phonon processes of the silicon-vacancy centre in diamond, *New J. Phys.* **17**, 043011 (2015).
- [48] Y. Zhou, A. Rasmita, K. Li, Q. Xiong, I. Aharonovich, and W.-b. Gao, Coherent control of a strongly driven silicon vacancy optical transition in diamond, *Nat. Commun.* **8**, 14451 (2017).
- [49] C. Weinzettl, J. Görlitz, J. N. Becker, I. A. Walmsley, E. Poem, J. Nunn, and C. Becher, Coherent Control and Wave Mixing in an Ensemble of Silicon-Vacancy Centers in Diamond, *Phys. Rev. Lett.* **122**, 063601 (2019).
- [50] L. J. Rogers, K. D. Jahnke, M. H. Metsch, A. Sipahigil, J. M. Binder, T. Teraji, H. Sumiya, J. Isoya, M. D. Lukin, P. Hemmer, and F. Jelezko, All-Optical Initialization, Readout, and Coherent Preparation of Single Silicon-Vacancy Spins in Diamond, *Phys. Rev. Lett.* **113**, 263602 (2014).
- [51] X.-X. Li, B. Li, and P.-B. Li, Simulation of topological phases with color center arrays in phononic crystals, *Phys. Rev. Research* **2**, 013121 (2020).
- [52] C. Bradac, W. Gao, J. Forneris, M. E. Trusheim, and I. Aharonovich, Quantum nanophotonics with group IV defects in diamond, *Nat. Commun.* **10**, 5625 (2019).
- [53] M.-A. Lemonde, V. Peano, P. Rabl, and D. G. Angelakis, Quantum state transfer via acoustic edge states in a 2D optomechanical array, *New J. Phys.* **21**, 113030 (2019).
- [54] M. K. Bhaskar, D. D. Sukachev, A. Sipahigil, R. E. Evans, M. J. Burek, C. T. Nguyen, L. J. Rogers, P. Siyushev, M. H. Metsch, H. Park, F. Jelezko, M. Lončar, and M. D. Lukin, Quantum Nonlinear Optics with a Germanium-Vacancy Color Center in a Nanoscale Diamond Waveguide, *Phys. Rev. Lett.* **118**, 223603 (2017).
- [55] G. D. Fuchs, V. V. Dobrovitski, R. Hanson, A. Batra, C. D. Weis, T. Schenkel, and D. D. Awschalom, Excited-State Spectroscopy Using Single Spin Manipulation in Diamond, *Phys. Rev. Lett.* **101**, 117601 (2008).
- [56] B. B. Buckley, G. D. Fuchs, L. C. Bassett, and D. D. Awschalom, Spin-light coherence for single-spin measurement and control in diamond, *Science* **330**, 1212 (2010).
- [57] B. Pingault, J. N. Becker, C. H. H. Schulte, C. Arend, C. Hepp, T. Godde, A. I. Tartakovskii, M. Markham, C. Becher, and M. Atatüre, All-Optical Formation of Coherent Dark States of Silicon-Vacancy Spins in Diamond, *Phys. Rev. Lett.* **113**, 263601 (2014).
- [58] J. N. Becker, B. Pingault, D. Groß, M. Gündoğan, N. Kukharchyk, M. Markham, A. Edmonds, M. Atatüre, P. Bushev, and C. Becher, All-Optical Control of the Silicon-Vacancy Spin in Diamond at Millikelvin Temperatures, *Phys. Rev. Lett.* **120**, 053603 (2018).
- [59] G. Balasubramanian, P. Neumann, D. Twitchen, M. Markham, R. Kolesov, N. Mizuochi, J. Isoya, J. Achard, J. Beck, J. Tissler, V. Jacques, P. R. Hemmer, F. Jelezko, and J. Wrachtrup, Ultra-long spin coherence time in isotopically engineered diamond, *Nat. Mater.* **8**, 383 (2009).
- [60] D. D. Sukachev, A. Sipahigil, C. T. Nguyen, M. K. Bhaskar, R. E. Evans, F. Jelezko, and M. D. Lukin, Silicon-Vacancy Spin Qubit in Diamond: A Quantum Memory Exceeding 10 ms with Single-Shot State Readout, *Phys. Rev. Lett.* **119**, 223602 (2017).
- [61] P. C. Maurer, G. Kucsko, C. Latta, L. Jiang, N. Y. Yao, S. D. Bennett, F. Pastawski, D. Hunger, N. Chisholm, M. Markham, D. J. Twitchen, J. I. Cirac, and M. D. Lukin, Room-temperature quantum bit memory exceeding one second, *Science* **336**, 1283 (2012).
- [62] N. Bar-Gill, L. M. Pham, A. Jarmola, D. Budker, and R. L. Walsworth, Solid-state electronic spin coherence time approaching one second, *Nat. Commun.* **4**, 1743 (2013).
- [63] B. Li, P.-B. Li, Y. Zhou, J. Liu, H.-R. Li, and F.-L. Li, Interfacing a Topological Qubit with a Spin Qubit in a Hybrid Quantum System, *Phys. Rev. Appl.* **11**, 044026 (2019).
- [64] J. M. Taylor, P. Cappellaro, L. Childress, L. Jiang, D. Budker, P. R. Hemmer, A. Yacoby, R. Walsworth, and M. D. Lukin, High-sensitivity diamond magnetometer with nanoscale resolution, *Nat. Phys.* **4**, 810 (2008).
- [65] L. Thiel, Z. Wang, M. A. Tschudin, D. Rohner, I. Gutiérrez-Lezama, N. Ubrig, M. Gibertini, E. Giannini, A. F. Morpurgo, and P. Maletinsky, Probing magnetism in 2D materials at

- the nanoscale with single-spin microscopy, *Science* **364**, 973 (2019).
- [66] S. D. Bennett, N. Y. Yao, J. Otterbach, P. Zoller, P. Rabl, and M. D. Lukin, Phonon-Induced Spin-Spin Interactions in Diamond Nanostructures: Application to Spin Squeezing, *Phys. Rev. Lett.* **110**, 156402 (2013).
- [67] K. V. Kepesidis, M.-A. Lemonde, A. Norambuena, J. R. Maze, and P. Rabl, Cooling phonons with phonons: Acoustic reservoir engineering with silicon-vacancy centers in diamond, *Phys. Rev. B* **94**, 214115 (2016).
- [68] Y.-F. Qiao, H.-Z. Li, X.-L. Dong, J.-Q. Chen, Y. Zhou, and P.-B. Li, Phononic-waveguide-assisted steady-state entanglement of silicon-vacancy centers, *Phys. Rev. A* **101**, 042313 (2020).
- [69] B. Li, X. Li, P. Li, and T. Li, Preparing squeezed spin states in a spin-mechanical hybrid system with silicon-vacancy centers, *Adv. Quantum Technol.* **3**, 2000034 (2020).
- [70] P. Ouartchaiyapong, L. M. A. Pascal, B. A. Myers, P. Lauria, and A. C. Bleszynski Jayich, High quality factor single-crystal diamond mechanical resonators, *Appl. Phys. Lett.* **101**, 163505 (2012).
- [71] M. J. Burek, N. P. de Leon, B. J. Shields, B. J. M. Hausmann, Y. Chu, Q. Quan, A. S. Zibrov, H. Park, M. D. Lukin, and M. Lončar, Free-standing mechanical and photonic nanostructures in single-crystal diamond, *Nano Lett.* **12**, 6084 (2012).
- [72] Y. Tao, J. M. Boss, B. A. Moores, and C. L. Degen, Single-crystal diamond nanomechanical resonators with quality factors exceeding one million, *Nat. Commun.* **5**, 3638 (2014).
- [73] M.-A. Lemonde, S. Meesala, A. Sipahigil, M. J. A. Schuetz, M. D. Lukin, M. Loncar, and P. Rabl, Phonon Networks with Silicon-Vacancy Centers in Diamond Waveguides, *Phys. Rev. Lett.* **120**, 213603 (2018).
- [74] S. Meesala, Y.-I. Sohn, B. Pingault, L. Shao, H. A. Atikian, J. Holzgrafe, M. Gündoğan, C. Stavrakas, A. Sipahigil, C. Chia, R. Evans, M. J. Burek, M. Zhang, L. Wu, J. L. Pacheco, J. Abraham, E. Bielejec, M. D. Lukin, M. Atatüre, and M. Lončar, Strain engineering of the silicon-vacancy center in diamond, *Phys. Rev. B* **97**, 205444 (2018).
- [75] J. R. Schrieffer and P. A. Wolff, Relation between the Anderson and Kondo Hamiltonians, *Phys. Rev.* **149**, 491 (1966).
- [76] D. J. Wineland, J. J. Bollinger, W. M. Itano, and D. J. Heinzen, Squeezed atomic states and projection noise in spectroscopy, *Phys. Rev. A* **50**, 67 (1994).
- [77] D. J. Wineland, J. J. Bollinger, W. M. Itano, F. L. Moore, and D. J. Heinzen, Spin squeezing and reduced quantum noise in spectroscopy, *Phys. Rev. A* **46**, R6797 (1992).
- [78] M. Perarnau-Llobet, A. González-Tudela, and J. I. Cirac, Multimode Fock states with large photon number: Effective descriptions and applications in quantum metrology, *Quantum Sci. Technol.* **5**, 025003 (2020).
- [79] R. Nelz, P. Fuchs, O. Opaluch, S. Sonusen, N. Savenko, V. Podgursky, and E. Neu, Color center fluorescence and spin manipulation in single crystal, pyramidal diamond tips, *Appl. Phys. Lett.* **109**, 193105 (2016).
- [80] P. Ouartchaiyapong, K. W. Lee, B. A. Myers, and A. C. B. Jayich, Dynamic strain-mediated coupling of a single diamond spin to a mechanical resonator, *Nat. Commun.* **5**, 4429 (2014).